Technical Paper

Cyber coordinated simulation for distributed multi-stage additive manufacturing systems

Hongyue Sun[a], Giulia Pedrielli[b,*], Guanglei Zhao[c], Chi Zhou[a], Wenyao Xu[d], Rong Pan[b]

[a] *Industrial Engineering, University at Buffalo, Buffalo, NY, 14260 USA*
[b] *School of Computing Informatics & Decision Systems Engineering, Arizona State University, Tempe, AZ, 85251 USA*
[c] *Alta Devices Inc. Sunnyvale, CA 94085 USA*
[d] *Computer Science and Engineering, University at Buffalo, Buffalo, NY, 14260 USA*

ARTICLE INFO

ABSTRACT

Additive Manufacturing (AM) processes have been increasingly used to manufacture energy storage products with dedicated material preparation and post-processing stages to enhance product properties. Most researchers focus on selecting materials and improving processes, yet the system modeling and management has not been investigated so far. This paper extends the conventional single-stage AM processes to multi-STage distRibutEd AM (STREAM) systems. In STREAM, a batch of material produced at the pre-processing stage is jointly consumed by distributed AM printers, and then the printed parts are collected for the post-processing stage. Modeling and managing such complex systems have been challenging. We propose a novel framework for "cyber-coordinated simulation" to manage the hierarchical information in STREAM. This is important because simulation can be used to infuse data into predictive analytics, thus providing guidance for the optimization and control of STREAM operations. The proposed framework is hierarchical in nature, where the single-stage, multi-stage, and distributed productions are modeled through the integration of different simulators. We demonstrate the proposed framework with simulation data from Freeze Nano Printing (FNP) AM for the fabrication of energy storage products.

1. Introduction

Energy storage products are requesting both high energy density and high power density, but most of the existing processes are unable to manufacture energy products with both properties [1]. Freeze Nano Printing (FNP) is a novel 3D printing process that has the potential to satisfy these two requirements simultaneously. FNP seamlessly integrates inkjet printing, rapid freezing and freeze casting in order to fabricate multi-scale multi-functional porous structures [2,3]. Fig. 1 shows a demonstration of the FNP process. Differing from other AM processes, where materials are heated up, the FNP prints nano-materials in a solution by rapidly freezing the solution into a solid (Fig. 1). In specific, the aqueous nano-material suspensions are usually centrally prepared (Step 1) and loaded into reservoirs for electrode and electrolyte materials. The materials are selectively solidified in cryogenic environment (Step 2) during printing, where water serves as support media to hold the overhang features. The 3D printed ice structure is heat-treated by further freezing and then the ice is removed by

sublimation, leaving a porous structure (Step 3). The resulting body can either be used as is or be further annealed or sintered, depending on the properties of the materials (Step 4). Compared to existing AM processes, the FNP has advantages of: (1) Multi-scalability: The macroscopic structures are controlled by inkjet printing, while the microscopic features are controlled by freeze casting. (2) Enhanced integrity: Nano-material constructs with high integrity are formed by hydrogen bonding and $\pi - \pi$ stacking, overcoming the delamination issues widely seen in existing AM processes [2,3].

As shown in Fig. 1, the performance of FNP products depend not only on the printing stage in Step 2, but also on the pre-processing material preparation and post-processing thermal annealing stages. In addition, while the operations in pre-processing and post-processing stages are often centralized to achieve economies of scale, the main manufacturing stage, FNP, is envisioned to be distributed. This is because all 3D printers can fabricate customized individual parts and the production can be located closer to customers to shorten the supply chain. Therefore, the system has a batch of materials consumed by
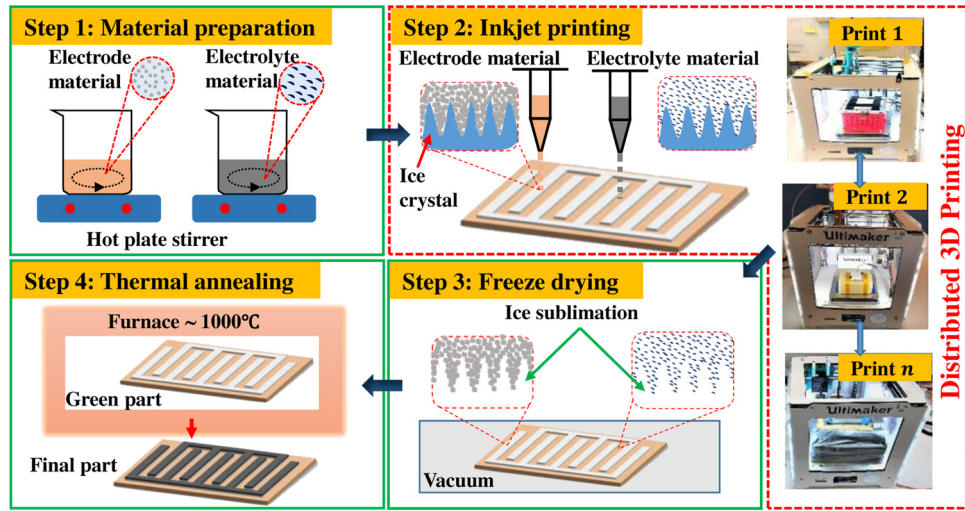
Fig. 1. diagram of the proposed freeze nano printing STREAM system.

distributed printers to fabricate energy products, which are annealed in a centralized furnace. We call such a system a multi-STage distRibutEd Additive Manufacturing (STREAM) system. The common properties of STREAM are: (1) a batch of raw material is prepared at a centralized location; (2) multiple AM machines, usually distributed in various locations, jointly consume the raw material for product fabrication; and (3) the fabricated products are transited to a centralized location for post-processing (e.g., support removal, sintering, annealing).

STREAM is a Cyber-Physical System (CPS) whose performance is intricately associated with local processes and interactions among these processes. For instance, the thermal management (thermal distribution and waiting time among layers for sufficient freezing and solidification) in the printing process plays a vital role. This is because the spatial and temporal thermal behavior governs both the macro-structure (geometry, dimension and surface quality) and micro-structure (pore size, density and morphology), which consequently affect the process quality, productivity and product functionality [4]. In addition, the post-processing (such as annealing) will affect the final product's geometry and properties, given a product printed from FNP. Currently, researchers only focus on optimizing the material selection and printing [2,3], but did not consider the interactions among multiple stages. In general, manufacturing processes in STREAM are usually analyzed/ planned locally in industry, resulting in a limited global performance [5,6]. The interaction among the processes is an important but much less investigated area. How to keep track of the STREAM system as a synergy poses significant challenges yet a great opportunity for the entire system optimization. CPS technologies have the potential to significantly and positively impact these manufacturing systems [7,8]. However, as pointed out in [9], "much literature effort has been put on technological characterization, while there is a lack of knowledge on the operations management characterization to manage such new systems". Some pioneer work has demonstrated some operation case studies, for instance, [8] provided Cloud-based Distributed Process Planning, which is a joint effort between KTH and Sandvik, Sweden, for cloud-based distributed and adaptive process planning. In this work, we investigate the system operation in a new FNP STREAM.

Two approaches for characterizing system operation are physical models or simulation models. Conventionally, physical based models are widely used to keep track of a manufacturing process. The physical based models have the advantage of interpretability from the system physics and can capture the process accurately after calibration [10]. However, when the system is complex like STREAM, an accurate physical model for the entire system is not yet available. Discrete Event Simulation (DES) can be used for such scenarios. However, STREAM poses significant challenges for DES since multiple distributed processes

take place, and it is extremely challenging to manage the DES so that it is reflective of the processes. In this work, we integrate the physical model and DES by cyber coordination to tackle this problem. It is worth noting that the STREAM structure is widely encountered in manufacturing systems and beyond. For instance, in the aero-engine coating process, the spraying particles are melted and propelled to the engine surface for surface protection [11]. The quality of the coating is highly dependent on the particle properties, such as uniformity, purity. Meanwhile, the coated surface will be trimmed before putting into service. The proposed cyber-coordinated simulation framework helps the system integration and operation excellence, and is widely applicable to these systems.

In this study, we demonstrate the cyber-coordinated simulation with FNP, and consider the hierarchical information flow at the local printing, multi-stage and STREAM levels. At the local FNP level, a physical model is used for describing the local printing process. However, the physical model is time-consuming to be executed, and we therefore build an emulator for the physical model. In particular, we are interested in: (1) the non-uniformity of the droplet thermal distributions, which will affect the macro-structure and micro-structure of the product; and (2) processing time, which is the summation of printing time and waiting time among layers. The thermal non-uniformity and processing time separately reflect the product quality and productivity, and will be modeled with material properties and printing process parameters in a multi-response Gaussian Process (GP) emulator. It should be noted that, in this paper, our focus is on proposing a cyber-coordinated simulation framework for the production control of the FNP process. In the future, we will study the tests such as the charge and discharge tests, since the physical models describing them are not well established and therefore it is very challenging to build simulators for them. At the production level, a DES is developed to generate adequate system sizing, loading rules, and sequencing decisions at different production stages. The system level simulator and the local level simulator will exchange the production scheduling information (from system to local production) and the quality information obtained for each part type (from local production to system). The main objective of the system simulation is to investigate the inter-dependencies among stages rather than modeling the process dynamics of the FNP.

The remainder of this paper is organized as follows. We review the related topics in Section 2. Section 3 outlines the cyber-coordinated simulation framework. After that, the STREAM physical system and cyber system are described in Sections 3.1 and 3.2, respectively. We then perform the simulation in Section 4, and demonstrate the proposed framework in Section 5 based on the simulation. Finally, we draw conclusion in Section 6.

2. Related literature

2.1. Energy-AM system

Due to the increasingly limited availability of fossil fuels and ever increasing growth in energy demand, there is an urgent need to develop next-generation high-power energy storage systems [12,13]. However, there are two major barriers for the existing fabrication approaches. First, as pointed out by the U.S. Defense Logistics Agency, the current energy storage devices have either high power density or high energy density, but not both [1]. Second, the current energy storage devices cannot meet the flexible design requirements from wearable sensors, etc. [14]. Benefiting from a large surface area, graphene aerogel supercapacitors have the advantage of high power and energy density with low weight ratio. These super capacitors are considered to be one of the most promising directions for energy storage devices [15]. However, the recent successful methods can only produce continuous films with no control over geometry and position. AM can selectively deposit multi-functional materials at specific locations in a controlled manner to form complex object [16–20], and this unique property makes AM one of the best candidates for fabricating engineered graphene supercapacitors, and has been broadly applied to fuel cells, batteries, hydrogen, solar cells, etc. [21]. FNP is a novel AM process that possesses high scalability and enhanced integrity [2,22], as introduced in Section 1. Currently, FNP is at niche stage, fabricating products with "tailored macro-architectures is still a significant challenge" [23]. There is a need to study the processes and systems for the product optimization. In particular, the thermal behavior is the most important factor in FNP, for both quality and productivity. Some endeavors have been spent to build physical models to describe the thermal behavior during the printing process [24–27]. These physical models can be predictive of the local processes, but cannot handle the continuous production system of STREAM structure. In this paper, we propose a novel cyber-coordinated simulation framework to systematically study the multi-stage and distributed processes in FNP, and improve the energy products fabrication quality and productivity.

2.2. STREAM system simulation

Concerning the manufacturing system, both analytical models (e.g., stochastic processes, differential equations) and Discrete Event Simulation have been widely adopted [28,29]. In particular, DES has shown very powerful for the analysis of the performance of automotive and assembly lines of arbitrary complexity [30,31]. As reviewed in [32], DES was classified into three general classes of manufacturing system design, manufacturing system operation, and simulation language/package development. This paper revealed a shift from design to operation in the literature, due to the increase of computational power and computer memory. For instance, [33] used DES for the scheduling of hydraulic valves production in a machining job-shop. [34] claimed that there is a lack of simulations for "analysis of the manufacturing process and integration with other dependable features such as production chains and the facility environment", and built a holistic simulation of a manufacturing facility considering machines, manufacturing process chain and built environment to understand the interaction between materials, energy and resource flows. In summary, DES can be used to capture the system heterogeneity (caused by distributed machines) and dynamics. Moreover, the machine assignment, resource tracking, etc. can be considered in the DES [35,36]. However, DES for STREAM has not been developed yet. One major aspect to consider when modeling STREAM is the presence of physical mechanisms/models that are adopted to emulate the physical freeze casting process and the system level dynamics which is mainly determined through events [37,38]. In principle, we need to coordinate the physical models characterizing the single job processing, and the system level dynamics mimicking the interaction among several machines

processing jobs at different stages. In this paper, in an attempt to achieve computational efficiency, and to supply the user the possibility to embed optimization within the simulation code, we will develop an event-based implementation of the system dynamics, where we *synchronize* the physical model(s) and the system level dynamics by triggering events that require to start the execution of the process model. Once the process model execution is over then an event is scheduled within the system simulator. Using DES for system level modeling is a choice justified by the ample literature and the modeling flexibility (e.g., no assumptions are required) that DES provides [28].

2.3. Contribution

This paper presents STREAM and shows the details of its development and testing in FNP. The FNP STREAM system studied herein uses physical models to represent the thermal distribution during the manufacturing process, a major determinant for the quality of the manufactured products. In order to allow for the system performance evaluation to run efficiently and, potentially, in real time, we develop a learning structure that uses physical simulations and potentially real data to construct a surrogate heat transfer model using a multi-response GP model. This GP-based emulator allows to quickly generate heat transfer information, and subsequently compute the processing time and printing failure. This information is integrated with the system level simulation model, which is implemented as event-based simulator. In order to enable such an integration, we extend the Event Relationship Graph formalism, proposed for the first time in [39], by creating new event types that allow to run the emulator. The major contributions of the proposed framework are:

1 STREAM cyber-coordinated simulation framework. STREAM is highly integrated at multiple levels, and it is extremely challenging to achieve the robust and efficient decision-making for quality and productivity control. The cyber-coordinated simulation transforms FNP and energy-AM field to unprecedented quality and productivity, and it can be applied to other cyber manufacturing systems.
2 Multi-response emulation of physical models. The complex physical phenomena in FNP can be described by physical models with multiple characteristics, but the computation of these physical models is time consuming. We therefore use a multi-response GP model to emulate these physical models, which can achieve the efficient and accurate prediction for new printing jobs.
3 Multi-level simulation for STREAM. We build a system level simulator for a large scale STREAM. In order to achieve computational efficiency, we chose the Discrete Event Simulation paradigm. Our system-level Discrete Event Model, based on Event Relationship Graphs, is synchronized with the physical process simulation by means of the processing time, which is set to be equal to the termination time for the numerical model, and the thermal profile resulting from the physical model that is responsible for deciding whether to scrap the produced job.

We test the physical and the integrated simulators over several production scenarios where incoming jobs have different geometries and are characterized by different manufacturing conditions leading to different failures during the FNP. We observe the impact of resource allocation and server capacity allocation on the cycle time and work in progress. We believe that this study will form the basis for the implementation of more distributed AM systems.

3. STREAM framework

As shown in Fig. 2, the STREAM framework consists of the physical system and the cyber-coordinated simulators. Section 3.1 introduces the FNP physical system that unlocks exotic material properties by
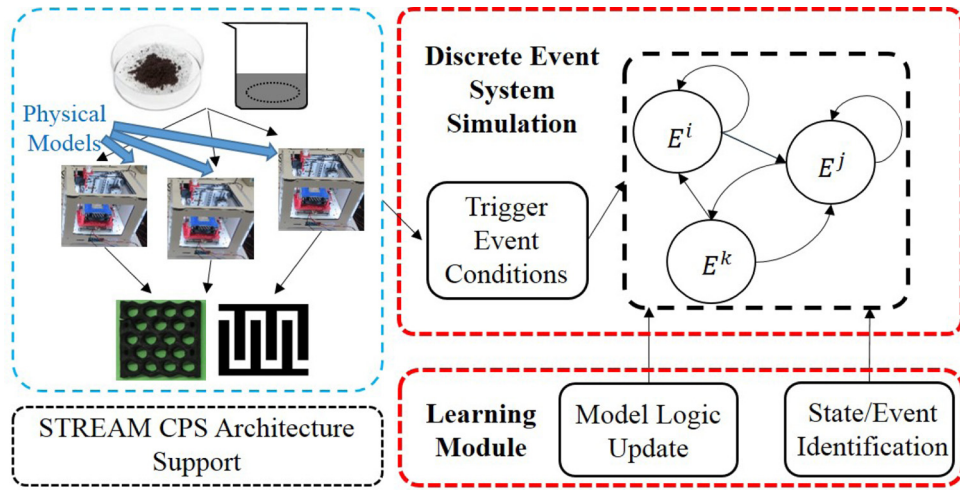
Fig. 2. STREAM cyber-coordinated simulation framework.

combining inkjet printing and freeze casting to print multi-scale multi-functional porous structures. The physical system to be built is a STREAM testbed for FNP energy-AM process. As a test case, dedicated design families of energy storage products (i.e., super-capacitors in Fig. 1) will be fabricated by energy-AM through simulation studies. Section 3.2 introduces the cyber system to be built in this work, which consists of multi-resolution distributed cyber simulators. These simulators will capture the manufacturing activities at single- and multi-stage processes, and the whole STREAM production system. The system dynamics during the simulation will be checked to guarantee the simulators are synchronized with the physical system.

3.1. The STREAM physical system

3.1.1. Printing system setup

The physical setup used in this paper is shown in Fig. 3a. A personal computer controls the whole system, including the three-axis motion driving system, material jetting system, temperature and pressure control system. Besides, the computer also stores the software that can

Fig. 3. (a) and (b) 3D printing graphene aerogel, 3D printed (c) truss structure and (d) 2.5 D structure on caltkin and (e) graphene aerogel with various wall thickness [2].

import 3D digital model and convert them into machine commands for the motion trajectory, material extrusion and other process parameters. The material jetting system consists of a pressure regulator, multiple material reservoirs, and piezo-based jetting devices. A temperature control system is applied to the print head such that the temperature of the material is constant and just above the melting point in order to keep reliable printing property. A two-nozzle platform is setup to print graphene and supporting material (ice), as shown in Fig. 3b. The whole system was placed in a freezer with the inside temperature well below the material's freezing point.

For inkjet printing, the graphene nanomaterial is hydrophobic and thus segregates in water even at very low concentration unless surfactants added for their surfaces are functionalized. The segregation of graphene leads to the nozzle clogging and thus severely affects the printability. Due to the presence of hydrophilic functional groups, Graphene Oxide (GO) is hydrophilic and can be easily dispersed in water at relatively high concentrations. Although GO is not electrically conductive, it can be thermally, chemically and photo-thermally reduced to graphene. Based on the excellent properties stated above, GO is suitable to serve as raw material. Low concentration (10mg/ml) aqueous GO ink was selectively ejected onto an aluminum platform with a certain amount of flow rate and moved following a predefined path. The ink is then frozen through the heat conduction with the platform and heat convection with the ambient. During the frozen process, the phase changing and separation can force the non-freezable solid nanomaterials (i.e., GO) to accumulate between the growing ice crystals. The nanomaterials trapped by the ice crystals form bridges between the crystals. If the loading of nanomaterial is enough, the entrapped nanomaterials will form a continuous 3D network molded by crystals. The 3D printed "green" part will then be freeze dried and the water will be removed to achieve the final graphene aerogel (GA) with porous structures. Fig. 3c-3 e shows multiple 3D printed GA structures. The interested readers are referred to our previous work for the detailed explanation of the 3D printing GA process [2].

To scale up the production, multiple printing systems described above could be allocated in various locations for the energy products printing. As discussed in Section 1, the STREAM physical system to be tested in the simulation consists of (1) pre-processing material preparation, which takes around 5 hours for a batch of 1000 ml; (2) FNP for 3D printing, the printers have a printing area of dimension $10cm \times 10cm$, and a printer can sequentially print multiple jobs. If multiple jobs are assigned to a printer, they can only be aligned within the same layer. Furthermore, there should be some spacing among the aligned parts. Here, we assume a 80% space utilization for the printing areas of the printers; (3) post-processing sintering, the sintering will
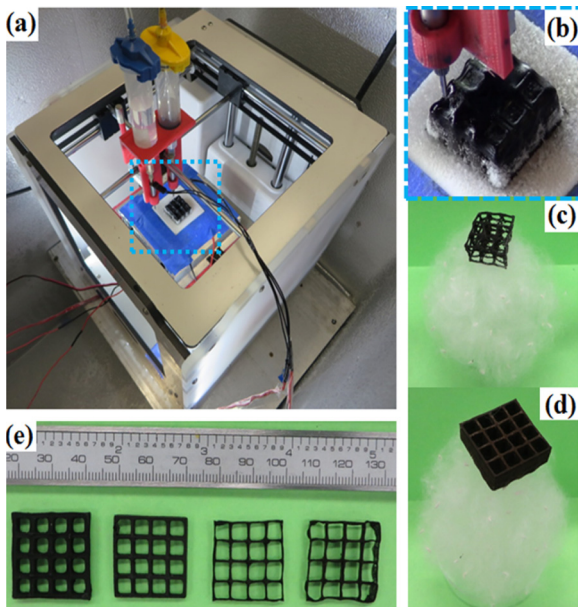
take 24 hours. The sintering furnace working dimension is $30cm \times 30cm$, and again, only one layer of the parts can be aligned in the furnace. We assume a space utilization rate of 80% for the furnace. It is very challenging to build and study such a STREAM system due to the complicated system structure and dynamics. In the following, we describe the proposed cyber-coordinated simulation framework for STREAM analysis.

3.2. The STREAM cyber system: printing process modeling and simulation

FNP integrates inkjet printing and freeze casting, and therefore has sophisticated heat transfer mechanism that affects the process performance (e.g., geometry and integrity). In particular, the freezing rate, which affects material bonding and process productivity, is governed by the heat transfer between the new material, frozen material, and environment temperature. As shown in Fig. 1 and Fig. 3, in the printing process, the materials are printed in a drop-on-demand (DoD) mode, in which discrete droplets are deposited onto the designed locations. The deposited inks, with an initial temperature of $5\ ^oC$ then solidify in a short time due to the heat conduction with the heat sink under build bed and heat convection with ambient (both -20^oC in this work). 3D parts are built layer by layer. After each layer, the nozzle waits until the entire layer solidifies before building a new layer on its top, in order to ensure the layer is cold enough to stand under the upcoming heat impulse (i.e., results in waiting time after each layer). We will use physical model and its emulator to describe the above phenomena in the FNP process, which is important for the printing process and entire STREAM production control.

In particular, we modified the heat transfer models from [40] for the energy products shown in Fig. 4. In the simulation, an element represents a droplet and the heat transfers are well depicted by computing thermal condition of each element iteratively through solving:

$$\nabla^2 T + \frac{\dot{q}}{k} = \frac{1}{\alpha}\frac{\partial T}{\partial t} \tag{1}$$

where T is temperature, $\dot{q}$ is the internal heat generation rate, k is material conductivity, and α is thermal diffusivity. There is no heat generation inside material, thus $\dot{q} = 0$.

With the "thermally small" theory [40], Eq. (1) can be simplified as the following iterative equation for solving the temperature history [40]:

$$T_{i+1} = (T_i - C_1)\exp\{[-C_2 \cdot \Delta t]\} + C_1 \tag{2}$$

where C_1 and C_2 are constants related to material properties and boundary conditions, and Δt is the time step. With appropriate materials properties and boundary condition inputs, explicit analytic solutions for thermal behavior of each element can be obtained from Eq. (2).

However, it is time-consuming to solve the model in Eq. (2) with an exact solver for energy products (for instance, the part in Fig. 4b took around 4 hours in Finite Element Analysis (FEA) to solve). To address this computational challenge, we propose a GP emulator of the physical model, so that the thermal characteristics can be predicted in near real time. The GP emulator will be constructed based on the material level characteristics and the process parameters. GP is widely used for physical model emulation and calibration [10,41,42], due to its capability to capture the nonlinear input-output relationships. In this work, we jointly model thermal non-uniformity and processing time via a multi-response GP model [41]:

$$\mathbf{y}_i = \boldsymbol{\eta}(\mathbf{x}_i) + \mathbf{e}_i \tag{3}$$

where $\mathbf{x}_i = (x_{1,i}, \cdots, x_{p,i})^T$ are the model inputs, $\mathbf{y}_i = (y_{1,i}, \cdots, y_{k,i})^T$ are the outputs, p and k are the number of inputs and outputs, respectively. $\boldsymbol{\eta}(\mathbf{x}_i)$ is the covariance for the outputs following GP, and $\mathbf{e}_i \sim N(0, \Sigma = \mathrm{diag}(\lambda_{s,0}^{-2}, \cdots, \lambda_{s,0}^{-2}))$ is the noise term. For the t-th output, the Gaussian kernel $\mathrm{Cov}(\mathbf{x}_i, \mathbf{x}_j) = \frac{1}{\lambda_{z,t}}\exp(-|\boldsymbol{\beta}_t^T(\mathbf{x}_i - \mathbf{x}_j)|_2) + \frac{1}{\lambda_{s,t}}$ is used, where $\mathbf{x}_i$ and $\mathbf{x}_j$ are two points in the parameter space, $\boldsymbol{\beta}_t$ is the scaling factor, $\lambda_{z,t}$ is the precision parameter captured by the model, and $\lambda_{s,t}$ is the precision parameter captured by the residual [41]. The parameter estimation can be performed using Markov Chain Monte Carlo (MCMC), see details in Section 5.

In this work, we are interested in the quality and productivity of the FNP STREAM system. The inputs to be used in the GP emulator are (1) specific heat (x_1), (2) frequency (x_2), (3) layer thickness (x_3), (4) interface heat coefficient (x_4), (5) element heat coefficient (x_5), and (6) super-capacitor droplet size (x_6), and the outputs to be used in the GP emulator are (1) thermal non-uniformity (y_1), which is calculated by follows: we count the time for a single element to fall from the initial temperature of 5^oC to -15^oC, and calculate the standard deviation of this temperature decrease rate among elements in a layer. The average of these layer-wise standard deviations is used to represent the overall part thermal non-uniformity; and (2) processing time (y_2), which is defined as the summation of waiting time and printing time. In Section 5, we will provide more details on the simulation data generation from the physical model, and GP emulator estimation and validation.

The emulator will interact with the DES for the STREAM operation optimization. In particular, to optimize the local process, one can find frequency and layer thickness that can yield uniform thermal distribution and appropriate processing time (the minimum time to allow sufficient freezing among layers). To optimize the global system, DES will synchronize the emulator and production simulators, which will be discussed next.

4. STREAM system simulation

4.1. Simulation principles

At the core of the proposed approach, we adopt Event Relationship Graphs (ERG). The ERG formalism can model any DES, and its formal relationship with Mathematical Programming, Petri Nets and Automata have been partially investigated in the literature [43–45].
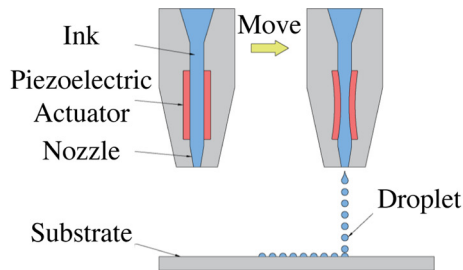
(a) Illustration of the Printing Process   **(b)** An Example of Printing Job

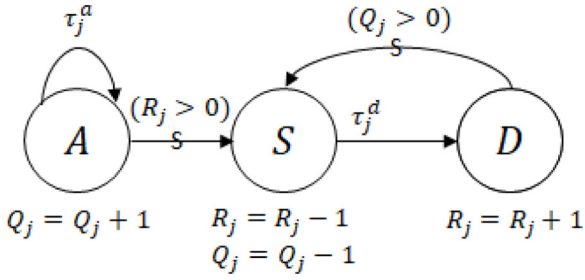**Fig. 4.** An illustration of the printing process and designed part.

Fig. 5. Example of event relationship graph.

Fig. 5 provides an example of ERG formalism to model a G/G/1 queue. The nodes A, S and D refer to the Arrival, Start, and Departure events, respectively. An arrival event can schedule another arrival event according to the inter-arrival time τ_{AA} (interpreted as either deterministic or as a realization from a random variable), and it increases the queue level $Q \leftarrow Q + 1$. An arrival event can schedule a start event if there is a free server (i.e, if $R > 0$, the arcs with "s" represent conditions). A start event reduces the number of free servers to $R = 0$ and the queue level $Q \leftarrow Q - 1$, and it schedules a departure event with a delay of τ_{SD}. The departure increases the number of free servers to $R = 1$ and it schedules a start in case there are jobs waiting in queue (i.e., $Q > 0$).

An hybrid version of the ERG in Fig. 5 can be obtained by modeling the events as Ordinary Differential Equation (ODE) or Partial Differential Equation (PDE). While such a modeling has not been proposed in the literature, we will extend ERGs in this paper to allow to specify continuous dynamics through differential equations, using the mechanics of event execution to trigger the simulation of the differential equation.

4.2. STREAM system model

Fig. 6 represents a simplified version of the ERG graph realized for the simulation of the STREAM system. We can see that, graphically, three main events blocks can be observed in the figure. The events with superscript "pre" refer to the pre-processing stage, while the events with superscript "am" refer to the additive manufacturing stage, and, finally, the superscript "post" refers to the set of events dedicated to the modeling of the dynamics of the post-processing stage.

We will separate the description of the model into two parts: First, we present the discrete event dynamics for pre- and post-process; then, we focus on the portion of the model dedicated to the additive manufacturing process in order to clearly explain the integration with the physical model.

4.2.1. Pre- and post-process stages

These stages have two types of events: the batching event (B_k^{pre}) and the departure event (D_k^{pre}). For the pre-process, we consider a total amount of raw material Δ and a utilization δ_i of raw material from each
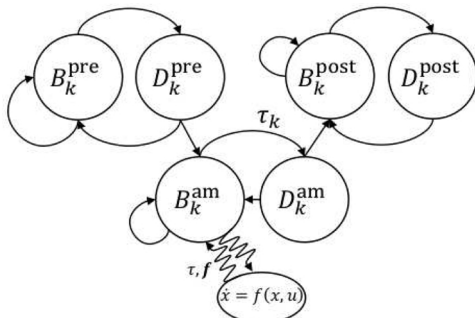

Fig. 6. ERG model for STREAM with physical model synchronization.

part type i. We assume a known product mix $\{\alpha_i\}_{i=1}^I$ where α_i represents the percentage of product of type i within the product mix and I is the number of considered part types. The simulation run length (the total number of produced jobs) is set to be N. At the pre-processing operation, the simulator receives as input a set of jobs to be produced, and, based on their characteristics, it generates the vector of expected material consumption, which we refer to as $B = \{b_1, b_2, ...\}$. The batch event is triggered if a pre-process resource is available and there is request for pre-process. At this point, it will process as much material as the capacity of the pre-process servers has and fill as many servers as available. So, we assume there are $k = 1, ..., M_{pre}$ servers that can perform the pre-process operation. The departure event is responsible for releasing the job to the AM stage. If an AM machine is available, then another batching event is scheduled to happen at any of the free servers at the AM stage (arc connecting D_k^{pre} to B_k^{am} in Fig. 6). We assume a stochastic uniform processing time for the pre-processing stage $U(t_{(pre,low)}, t_{(pre,up)})$. The post-processing stage is treated similarly; i.e., assume there are $k = 1, ..., M_{post}$ servers and a stochastic uniform processing time, $U(t_{(post,low)}, t_{(post,up)})$.

4.2.2. Additive manufacturing stage

For the printing stage, we have the same events defined for the previous stages. However, as represented in Fig. 6, the departure event B_k^{am} triggers the solution of the physical model (represented by the zigzag lines in Fig. 6). Specifically, the solution of the model leads to two inputs returned: the process time required for the set of jobs loaded into the machine and a vector **f** containing the indexes of the loaded jobs that resulted in a temperature profile outside of the allowed range. In such a scenario, the jobs need to be discarded and are not released to the post processing. The same information can be gathered from the GP-based emulator that approximates the physical model, presented in Section 3.2.

The process time is used to trigger the event D_k^{am}. As for the other stages, each job has a volume that is considered to compute the maximum number of jobs that are allowed in the same printing server. In particular, the jobs from the queue are chosen with the consideration of each printing machine's capacity. As a result, a set of jobs $J_i = \{j_1, j_2, ...\}$ is finally assigned to the i-th printing machine if it is free. The printing station is modeled as a parallel server with M_{am} resources.

There are two main elements of connection between the numerical simulation build to emulate the behavior of the physical process (section 3.2) and the system level simulation: (i) processing time which is a function of the frequency and droplet size, (ii) thermal non-uniformity that impacts the quality of the product. When the B_k^{am} is executed, the numerical simulation is started, then the length of the simulation $T_{i,k}$ for the i-th batch at the k-th printer (generally different for each printer and batch, this time is treated as a random variable), is saved. Another output that is saved is the batch thermal profile. In particular, a post-processing module (integrated within the numerical model) is responsible, based on the thermal profile to assess whether the thermal uniformity resulting from the simulation is such to cause a part failure. In case the profile is such to determine a part failure, then the job is flagged and the simulation model receives such information. At the end of the system simulation, we can know how many "failed jobs" were produced.

5. Numerical analysis

5.1. Physical model experiments and emulation

To evaluate the performance of the proposed method, we perform the simulation study of three sizes of the super-capacitor separately of dimensions 3.2×3.4 *mm*, 6.4×6.8 *mm*, and 9.6×10.2 *mm*, depending on x_6 in Table 1 . The ranges of other factors are shown in Table 1 . These ranges cover the typical working conditions of the FNP. To investigate the factors' effect on the printing process, a computer

Table 1
Physical model parameters and ranges.

Parameter	Unit	Lower/upper bound
Specific Heat x_1	J/kg.K	3375 / 3450
Frequency x_2	Hz	50 / 500
Layer Thickness x_3	mm	0.02 / 0.08
Interface Heat Coefficient x_4	W/m^2.K	150 / 400
Element Heat Coefficient x_5	W/m^2.K	60 / 120
Droplet Size x_6	mm	0.1 / 0.3

design of experiments of $n = 60$ runs is generated from stratified Latin hypercube design using min-max criterion [46]. In this computer experiment, the stratified design is used since x_1, x_2, x_4 and x_5 can take continuous values in the range shown in Table 1, while x_3 and x_6 take the value in three levels: 0.02, 0.05, and 0.08 mm, and 0.1, 0.2 and 0.3 mm, respectively, controlled by the signal to the piezo. The Latin hypercube design can have a good coverage of the design space [46].

As discussed in Section 3.2, the multi-response GP model is used to model the thermal non-uniformity and processing time as outputs with the factors in Table 1 as inputs [41]. Markov Chain Monte Carlo (MCMC) is used for model parameter estimation, where 3000 iterations are used for burn-in, and additional 10,000 iterations are used for the estimation. In particular, we use conjugate priors as hyperparameters, and follow [41] to get the posterior distribution for the GP emulator in Eq. (3). The model parameters mix well during the MCMC evaluations. We evaluate the model with five-fold Cross Validation (CV). In five-fold CV, we randomly divide the samples into five equally numbered pieces (each called a "fold"), and then iteratively use four out of the five folds to train the model and the left-out fold to evaluate the model prediction performance. The GP emulator prediction is achieved by sampling from the posterior distributions, see [41] on detailed derivations. Finally, we calculate the Normalized Root Mean Square Error (NRMSE) of thermal non-uniformity and processing time, bbased on the predicted value $\hat{y}_i$ and actual values y_i. NRMSE $= \frac{1}{\text{std}(\mathbf{y})}\sqrt{\frac{\sum_{i=1}^{n}(y_i - \hat{y}_i)^2}{n}}$ where $\mathbf{y} = (y_1, y_2, \cdots, y_n)^T$.

The prediction performance of the GP emulator is shown in Table 2. From the table, the emulator can accurately predict the outputs (with 3% of NRMSE). We then use all the 60 runs to build a GP emulator. The prediction for a new printing job is within 0.1s, which can afford the real-time simulation in DES. We integrate the emulator to the DES to understand the system operation, as investigated in Section 5.2.

5.2. System level analysis

The system level analysis considers a sequence of jobs to be processed by an FNP STREAM. The input information is: (1) sequence of jobs to be processed and their characteristics; (2) number of machines for each stage, and (3) capacity of each machine at each stage expressed in terms of volumetric capacity. Given that a job will have random processing times, we replicate the simulation experiments 100 times in order to statistically analyze the results, and we consider, across all the experimental conditions, a total of 600 jobs to produce.

Table 2
Normalized Root Mean Square Error (NRMSE) for the emulator prediction performance evaluation over five cv folds.

	Thermal non-uniformity	Processing time
CV1	0.0338	0.0225
CV2	0.0383	0.0228
CV3	0.0317	0.0272
CV4	0.0203	0.0173
CV5	0.0193	0.0195
Mean	0.0287	0.0219
Standard Error	0.0085	0.0037

5.2.1. Job Generation

In order to generate the jobs, we use the GP emulator trained above. Specifically, we vary the frequency, layer thickness and droplet size in the ranges in Table 1 while fixing the parameters related to the material properties at their mean levels for a fixed pre-processing batch. Given the parameter combination for a generated job, its material consumption and volume is known to the simulator for the design in Fig. 4(b). For the thermal non-uniformity and processing time, we sample 100 realizations from the posterior distribution of the multi-response GP emulator, and calculate the average of these 100 realizations. If a job's thermal non-uniformity is larger than a pre-defined threshold, the part is labeled as failed (i.e., failure label). The material, volume, processing time and failure label will be used in the experiments below.

5.2.2. Design of Experiments

In this analysis, we look into the cycle time for the jobs and the saturation of the machines. Our specific interest is to understand the impact of decisions related to the size of the printing machines and their number over the job performance. In order to perform such a study, we propose two main factors, i.e., the number of servers at each stage of the line, and the ratio of large to small printers in the AM step. This choice leads to the design in Table 3.

While the first three factors are intuitive, the last factor refers to the ratio, at the AM stage, between the number of servers with low volumetric processing capacity, against those with high volumetric capacity. In particular, the low capacity is defined based on the smallest processable job size $v_{\min}$, and the volume associated with the largest job size, i.e., $v_{\max}$. We assume that two alternative printing solutions are available, one offering a capacity $C_{\min} = 5 \cdot v_{\min}$ and the larger printer giving a capacity $C_{\max} = 5 \cdot v_{\max}$. As a result, given a specific configuration in terms of number of servers, if the solution we adopt is balanced, i.e., the last factor takes value [0.5, 0.5], then we will have half of the printers with capacity C_{min}, while the remaining will be large, i.e., will have capacity C_{max}.

Considering the conditions in Table 3, we have a total of 24 conditions, each to be replicated $N = 100$ times, for a total of 2400 experiments. The detailed experiments are shown in Table 4. Note that the same indexing for the conditions is used as x-axis in Fig. 7, Fig. 8, Fig. 9-Fig. 10.

5.2.3. Results

The waiting time at each stage of the line has been analyzed, as well as the cycle time by separating the jobs generated through the emulator in *small, medium*, and *large* sizes. Such a separation is operated by volume. More specifically, for each emulator generation, we take the minimum and maximum of the generated volume and create three uniform volume intervals and classify the jobs into three categories. This is important since we hypothesize that the decision on the balance between small and large AM machines can impact in a different way the different job categories.

Fig. 7 reports the waiting times across the different conditions for the pre-processing phase. We can notice that the pre-processing waiting time is only influenced by the number of resources at the pre-processing stage itself. This is reasonable due to the fact that the printing stage is the bottleneck of the system under all conditions. A recommendation would therefore be to maximize the capacity of the pre-processing stage

Table 3
Factors and corresponding levels for the system level analysis.

Factors	Levels		
# of pre-process servers	2	4	
# of FNP servers	6	12	
# of post-process servers	2	4	
Ratio small/large servers in FNP	[0.5, 0.5]	[1/3, 2/3]	[2/3, 1/3]

Table 4
Experimental conditions for system performance analysis [(**) b = [0.5,0.5], s = [2/3,1/3], l = [1/3,2/3]].

Condition	# pre	# post	# Printers	Ratio (**)
1	2	2	6	b
2	2	2	6	s
3	2	2	6	l
4	2	2	12	b
5	2	2	12	s
6	2	2	12	l
7	2	4	6	b
8	2	4	6	s
9	2	4	6	l
10	2	4	12	b
11	2	4	12	s
12	2	4	12	l
13	4	2	6	b
14	4	2	6	s
15	4	2	6	l
16	4	2	12	b
17	4	2	12	s
18	4	2	12	l
19	4	4	6	b
20	4	4	6	s
21	4	4	6	l
22	4	4	12	b
23	4	4	12	s
24	4	4	12	l

to avoid cumulating the jobs at the beginning of the process. Nonetheless, care needs to be paid to the effect on the waiting time at the printing stage.

Fig. 8(a) shows the much different situation at the printing stage, the bottleneck of the system. In particular, the worst performance in terms of waiting time for small parts is achieved (independently from the pre-process condition) when a low number of large printers is available. This is due to the fact that large volumes are loaded in the printer and the processing times get larger especially for small parts that, if processed individually would leave the system quickly. Due to the smaller processing time, the small parts see the efficiency maximized for the conditions with a large number of small printing devices. The situation is different for large volume jobs (Fig. 8(c)), where we observe how detrimental is the strategy with a small number of small resources, independently from the pre-processing settings. The same holds for medium sized jobs (Fig. 8(b)).

Concerning the waiting time at the last stage (Fig. 9), while it is apparent that the variance is influenced by the condition, the waiting times are basically 0 for all the conditions revealing the low impact of capacity increase at the post-processing level. This result is expected to due to the large capacity of the post-process and the shorter processing time.

Finally, the cycle time, as expected, resembles the bottleneck performance (Fig. 10). These results lead us to recommend a system design with balanced printers in order to preserve larger jobs without worsening the performance for smaller jobs.

6. Conclusion

In this paper, we present a novel STREAM framework for FNP, to scale up the energy storage products manufacturing. STREAM is a complex system encompassing several challenges. This paper proposes a cyber coordinated simulation framework to describe the system operations and enable the analysis of the system performance offline and, in principle, on the shop floor.

We present the physical system and the models that describe the fundamental process of thermal distribution. The physical models are very expensive and impractical to be adopted for performance evaluation/STREAM design offline, and, even more, for real time analytics
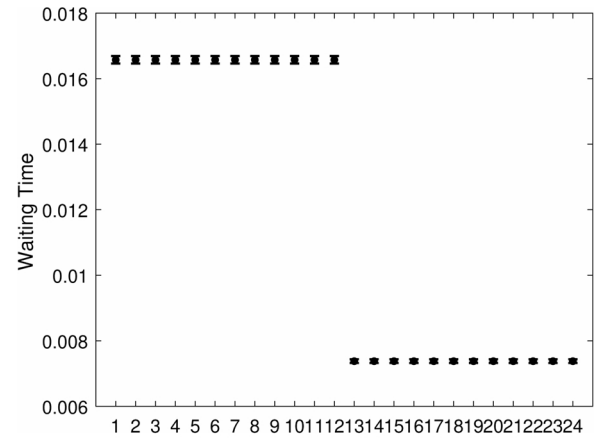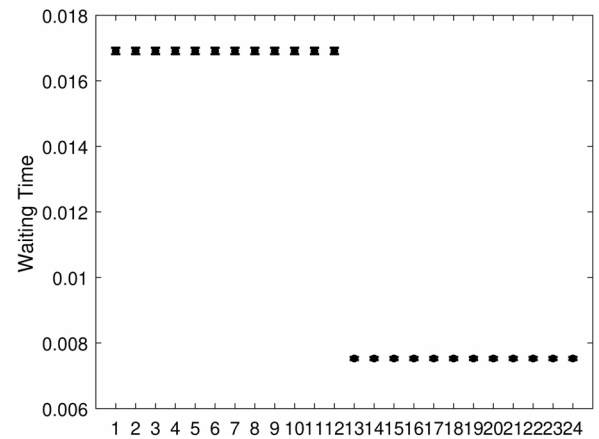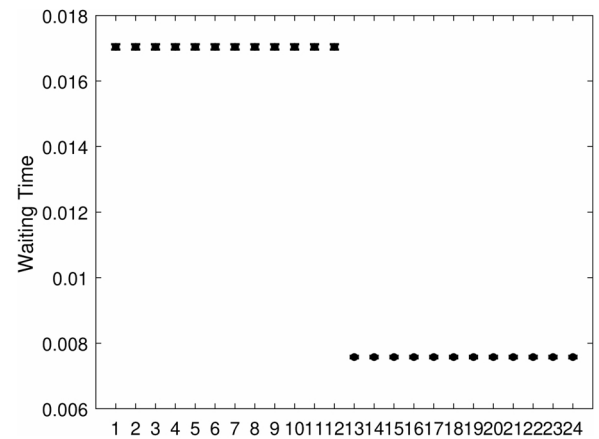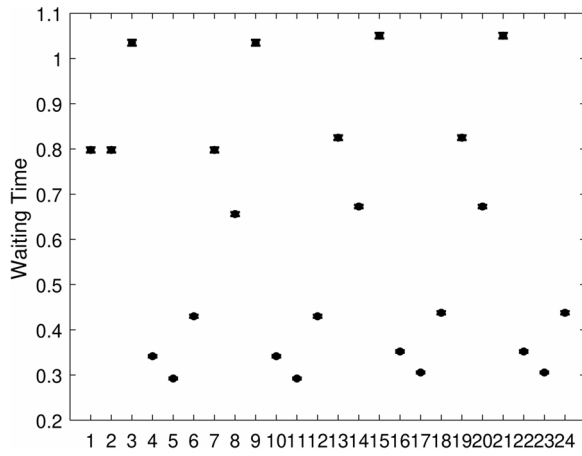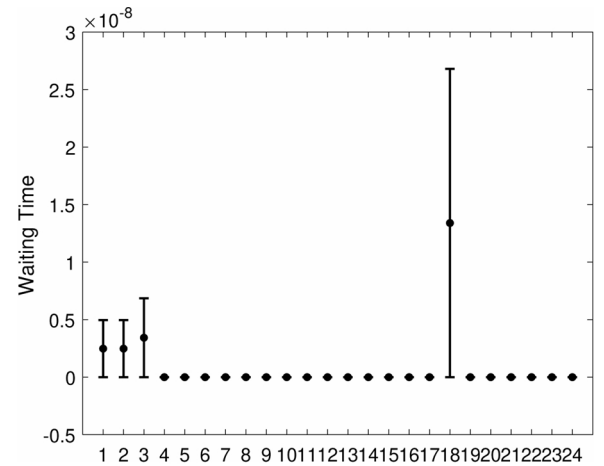

(a) Small Parts

(b) Medium Parts

(c) Large Parts

**Fig. 7.** Average waiting times for pre-processing across the experimental conditions.

purposes. In view of this challenge, and to make the framework usable in real time settings, an emulator is constructed to replace the time-consuming physical model. Specifically, the emulator is based on a multi-response Gaussian Process model, and can predict the energy product thermal non-uniformity and processing time accurately in near real time. The emulator not only can be trained from the physical laws, but it can be calibrated in the future from sensor information coming
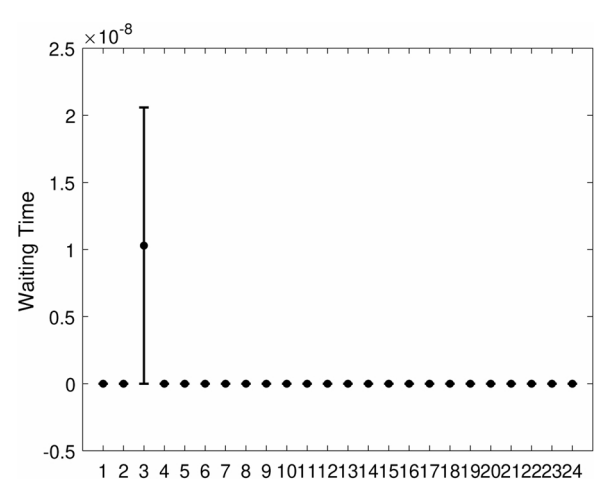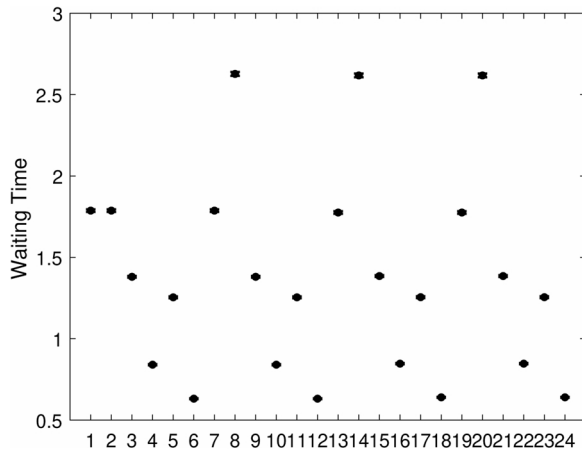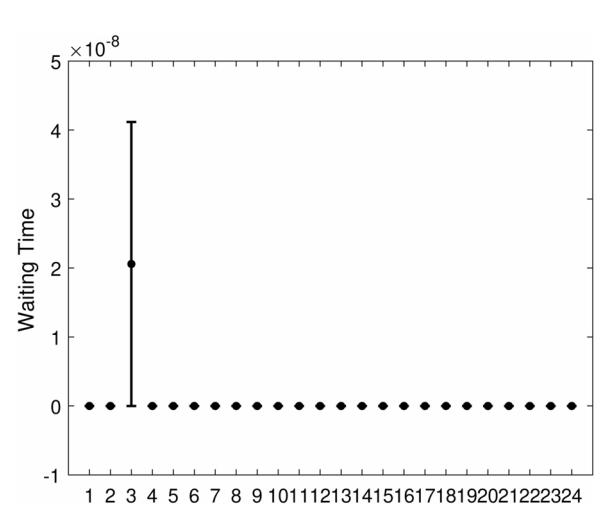
(a) Small Parts
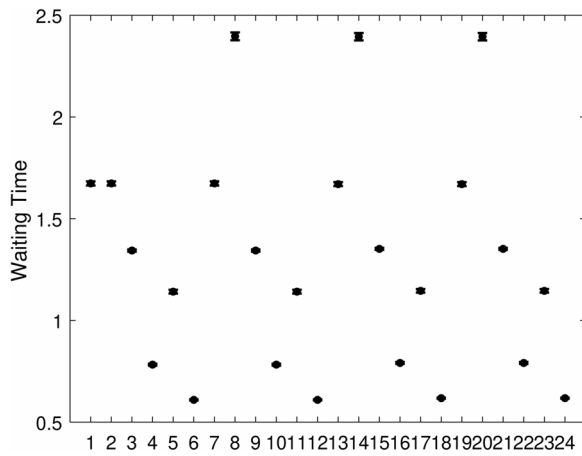
(b) Medium Parts

(c) Large Parts

Fig. 8. Average waiting times for printing phase across the experimental conditions.

(a) Small Parts

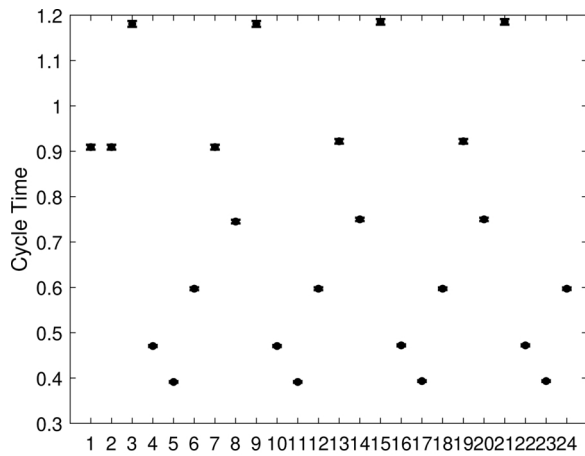**(b)** Medium Parts

(c) Large Parts

Fig. 9. Average waiting times for post-processing phase across the experimental conditions.

from the real system. The physical model as well as the emulator can be smoothly connected with the discrete event simulator that, with a novel extension from Event Relationship Graphs, exposes integration events that trigger the solution of the physical model or the bootstrap of the emulator allowing to simulate the processing of jobs through the pre-
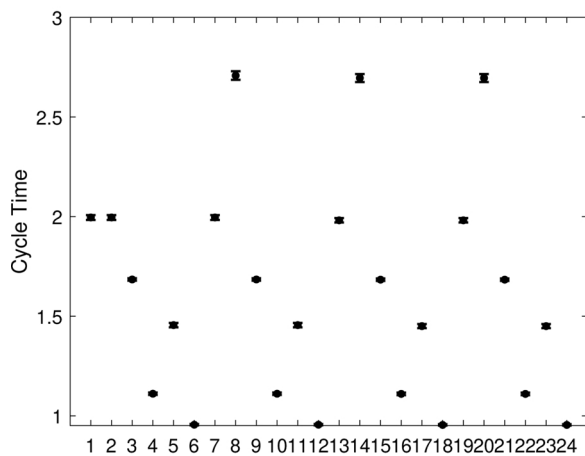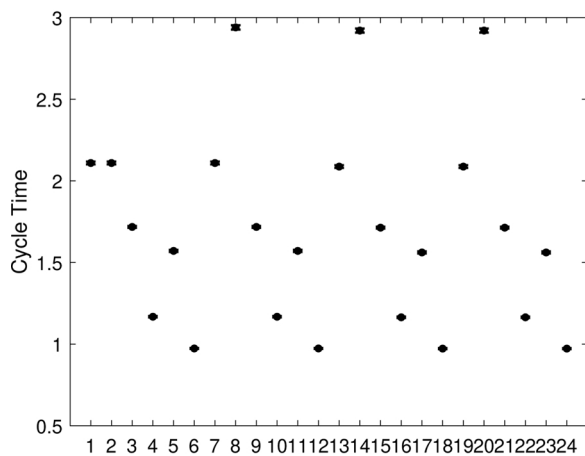
processing, post-processing and printing stages.

The numerical experiments show that a STREAM should be designed with large pre-processing capacity and with printing devices of

(a) Small Parts

(b) Medium Parts

(c) Large Parts

Fig. 10. Average cycle time across the experimental conditions.

variable capacity. In particular, solutions with a balanced number of small and large printing machines prevailed in our analysis. Nonetheless, it is critical to have a large number of printers. This further motivates to study networked STREAMs, i.e., production systems that are geographically dispersed.

The proposed framework can be applied to a wide range of scenarios

and benefit the related industries. The direct application of the proposed framework is the production control in FNP of energy products, which is expected to scale up the FNP production. Other applications include aero-engine surface coating where metal coating particles and coating process conditions need to be coherently analyzed and controlled [11], multistage assembly where multiple consecutive operations need to be jointly considered to arrive at the desired final geometry [47]. It is expected that seamlessly connecting these machines and systematically modelling and stimulating the multi-level interconnections will greatly enhance the local machine and system decision-making. The proposed cyber-coordinated simulation can be integrated into existing software and tools, such as Simio, to improve the production control accuracy and efficiency. In particular, the object oriented nature of Simio can be used to implement the desired connection with the process level models. It also has the potential to be integrated into new CPS platforms, such as GE Predix, IBM Watson Analytic.

In the future, we will deepen the connection of the discrete event simulator with real data coming from the physical system, by enabling the dynamically update of the model logic based on the functioning of the system. This is particularly important for geographically distributed STREAMs where portions of the system may be inactive at specific intervals of time and, based on the state information available in the cloud, the simulators should be able to adapt. In addition, other tests such as the charge and discharge tests will be investigated and integrated into the simulation framework.

Conflict of interest statement

The author declares that there is no conflict of interests to this work.

Declaration of Competing Interest

The authors report no declarations of interest.

Acknowledgment

References

[1] Johnson DC, Prieto AL. Three-dimensional lithium-ion batteries with interdigitated electrodes. Energy harvesting and storage: materials,devices, and applications IV, 8728. 2013. p. p872805.
[2] Zhang Q, Zhang F, Medarametla SP, Li H, Zhou C, Lin D. 3d printing of graphene aerogels. Small 2016;12(13):1702–8.
[3] Yan P, Brown E, Su Q, Li J, Wang J, Xu C, Zhou C, Lin D. 3d printing hierarchical silver nanowire aerogel with highly compressive resilience and tensile elongation through tunable poisson's ratio. Small 2017;13(38):1701756.
[4] Yang F, Zhao G, Zhou C, Lin D. Phase change materials (pcm) based cold source for selective freezing 3d printing of porous materials. Int J Adv Manuf Tech 2018;95(5–8):2145–55.
[5] Gaus T, Olsen K, Deloso M. Synchronizing the digital supply network (https://www2.deloitte.com/content/dam/insights/us/articles/4405_Synchronized-planning/DI_Synchronized-planning.pdf). 2018.
[6] Hanley T, Daecher A, Cotteleer M, Holdowsky J. The industry 4.0 paradox: Overcoming disconnects on the path to digital transformation (https://www2.deloitte.com/content/dam/Deloitte/cn/Documents/energy-resources/deloitte-cn-er-industry-4.0-paradox-overcoming-disconnects-en-full-report-190225.pdf). 2018.
[7] Mittal S, Khan MA, Romero D, Wuest T. A critical review of smart manufacturing & industry 4.0 maturity models: implications for small and medium-sized enterprises (smes). J Manuf Syst 2018;49:194–214.
[8] Wang L, Törngren M, Onori M. Current status and advancement of cyber-physical systems in manufacturing. J Manuf Syst 2015;37:517–27.
[9] Napoleone A, Macchi M, Pozzetti A. A review on the characteristics of cyber-physical systems for the future smart factories. J Manuf Syst 2020;54:305–35.
[10] Kennedy MC, O'Hagan A. Bayesian calibration of computer models. J R Stat Soc Series B Stat Methodol 2001;63(3):425–64.
[11] Sun H, Huang S, Jin R. Functional graphical models for manufacturing process

modeling. Ieee T Autom Sci Eng 2017;14(4):1612–21.

[12] Winter M, Brodd RJ. What are batteries, fuel cells, and supercapacitors?. 2004.

[13] Long JW, Dunn B, Rolison DR, White HS. Three-dimensional battery architectures. Chem Rev 2004;104(10):4463–92.

[14] González A, Goikolea E, Barrena JA, Mysyk R. Review on supercapacitors: technologies and materials. Renew Sust Energ. Rev 2016;58:1189–206.

[15] Arico AS, Bruce P, Scrosati B, Tarascon J-M, Van Schalkwijk W. Nanostructured materials for advanced energy conversion and storage devices. Materials for sustainable energy: a collection of peer-reviewed research and review articles from nature publishing group. World Scientific; 2011. p. 148–59.

[16] Tian X, Jin J, Yuan S, Chua CK, Tor SB, Zhou K. Emerging 3d-printed electrochemical energy storage devices: a critical review. Adv Energy Mater 2017;7(17):1700127.

[17] Beidaghi M, Gogotsi Y. Capacitive energy storage in micro-scale devices: recent advances in design and fabrication of micro-supercapacitors. Energy Environ Sci 2014;7(3):867–84.

[18] Areir M, Xu Y, Harrison D, Fyson J. 3d printing of highly flexible supercapacitor designed for wearable energy storage. Mater Sci Eng B 2017;226:29–38.

[19] Foster CW, Down MP, Zhang Y, Ji X, Rowley-Neale SJ, Smith GC, et al. 3d printed graphene based energy storage devices. Sci Rep 2017;7:42233.

[20] Bardpho C, Rattanarat P, Siangproh W, Chailapakul O. Ultra-high performance liquid chromatographic determination of antioxidants in teas using inkjet-printed graphene-polyaniline electrode. Talanta 2016;148:673–9.

[21] Zhakeyev A, Wang P, Zhang L, Shu W, Wang H, Xuan J. Additive manufacturing: unlocking the evolution of energy materials. Adv Sci 2017;4(10):1700187.

[22] Zhang F, Yang F, Lin D, Zhou C. Parameter study of three-dimensional printing graphene oxide based on directional freezing. J Manuf Sci Eng 2017;139(3).

[23] Zhu C, Liu T, Qian F, Han TY-J, Duoss EB, Kuntz JD, et al. Supercapacitors based on three-dimensional hierarchical graphene aerogels with periodic macropores. Nano lett 2016;16(6):3448–56.

[24] Zhao G, Lin D, Zhou C. Thermal analysis of directional freezing based graphene aerogel three-dimensional printing process. J Micro Nanomanuf 2017;5(1).

[25] Zhao G, Zhou C, Lin D. Tool path planning for directional freezing-based three-dimensional printing of nanomaterials. J Micro Nanomanuf 2018;6(1).

[26] Sui G, Leu MC. Thermal analysis of ice walls built by rapid freeze prototyping. J Manuf Sci Eng 2003;125(4):824–34.

[27] Bryant FD, Leu MC. Predictive modeling and experimental verification of temperature and concentration in rapid freeze prototyping with support material. J Manuf Sci Eng 2009;131(4):041020.

[28] Cassandras CG. Discrete event systems: modeling and performance analysis. CRC; 1993.

[29] Jin J, Shi J. State space modeling of sheet metal assembly for dimensional control. J Manuf Sci Eng 1999;121(4):756–62.

[30] Shi J. Stream of variation modeling and analysis for multistage manufacturing processes. CRC press; 2006.

[31] Mourtzis D, Doukas M, Bernidaki D. Simulation in manufacturing: Review and challenges. Procedia CIRP 2014;25:213–29.

[32] Negahban A, Smith JS. Simulation for manufacturing system design and operation: Literature review and analysis. J Manuf Syst 2014;33(2):241–61.

[33] Zhang M, Tao F, Nee A. Digital twin enhanced dynamic job-shop scheduling. J Manuf Syst 2020.

[34] Mawson VJ, Hughes BR. The development of modelling tools to improve energy efficiency in manufacturing processes and systems. J Manuf Syst 2019;51:95–105.

[35] Mourtzis D. Simulation in the design and operation of manufacturing systems: state of the art and new trends. Int J Prod 2020;58(7):1927–49.

[36] Jiang H, Qin S, Fu J, Zhang J, Ding G. How to model and implement connections between physical and virtual models for digital twin application. J Manuf Syst 2020.

[37] Henzinger TA. The theory of hybrid automata. Verification of digital and hybrid systems. Springer; 2000. p. 265–92.

[38] Grossman RL, Nerode A, Ravn AP, Rischel H. Hybrid systems. Springer; 1993.

[39] Schruben L. Confidence interval estimation using standardized time series. Oper Res 1983;31(6):1090–108.

[40] Zhao G, Zhou C, Lin D. Thermal analysis on directional freezing of nano aqueous suspensions in graphene aerogel 3d printing process. ASME 2016 11th international manufacturing science and engineering conference. 2016.

[41] Higdon D, Gattiker J, Williams B, Rightley M. Computer model calibration using high-dimensional output. J Am Stat Assoc 2008;103(482):570–83.

[42] Sun H, Luo S, Jin R, He Z. Ensemble engineering and statistical modeling for parameter calibration towards optimal design of microbial fuel cells. J Power Sources 2017;356:288–98.

[43] Savage EL, Schruben LW, Yücesan E. On the generality of event-graph models. Informs J Comput 2005;17(1):3–9.

[44] Schruben L. Simulation modeling with event graphs. Commun Acm 1983;26(11):957–63.

[45] Schruben L, Yucesan E. Complexity of simulation models a graph theoretic approach. Proceedings of 1993 winter simulation conference-(WSC'93). 1993. p. 641–9.

[46] Santner TJ, Williams BJ, Notz W, Williams BJ. The design and analysis of computer experiments. Springer; 2003.

[47] Liu J, Jin J, Shi J. State space modeling for 3-d variation propagation in rigid-body multistage assembly processes. Ieee T Autom Sci Eng 2009;7(2):274–90.